PCCP

Highly precise characterization of the hydration state upon thermal denaturation of human serum albumin using a 65 GHz dielectric sensor

Journal:	*Physical Chemistry Chemical Physics*
Manuscript ID	CP-ART-04-2020-002265.R1
Article Type:	Paper
Date Submitted by the Author:	10-Jul-2020

Complete List of Authors:	Shiraga, Keiichiro; RIKEN, Integrative Medical Sciences; Kyoto University Urabe, Mako; RIKEN Center for Integrative Medical Sciences Matsui, Takeshi; RIKEN Center for Integrative Medical Sciences Kikuchi, Shojiro; Hyogo College of Medicine Ogawa, Yuichi; Kyoto University,

Highly precise characterization of the hydration state upon thermal denaturation of human serum albumin using a 65 GHz dielectric sensor

Keiichiro Shiraga[a, b*] keiichiro.shiraga@riken.jp

Mako Urabe[a] mako.urabe@riken.jp

Takeshi Matsui[a] takeshi.matsui@riken.jp

Shojiro Kikuchi[c] skikuchi@hyo-med.ac.jp

Yuichi Ogawa[b] ogawayu@kais.kyoto-u.ac.jp

[a] RIKEN Center for Integrative Medical Sciences (IMS), Tsurumi, Yokohama, Kanagawa 230-0045, Japan

[b] Graduate School of Agriculture, Kyoto University, Kitashirakawa-oiwake, Sakyo, Kyoto 606-8502, Japan

[c] Department of Reverse Translational Research, Hyogo College of Medicine, Mukogawa, Nishinomiya, Hyogo 663-8501, Japan

* Corresponding author E-mail. keiichiro.shiraga@riken.jp

Abstract

Biological functions of proteins depend on harmonization with hydration water surrounding them. Indeed, dynamical transition of proteins, such as thermal denaturation, is slaved to changes in *mobility* of hydration water. However, its commitment during dynamical transition is yet to be fully understood, due to technical limitations in precisely characterizing the *amount* of hydration water. A state-of-art CMOS dielectric sensor consisting of 65 GHz LC resonators addressed this issue by utilizing the feature that oscillation frequency sensitively shifts in response to the complex dielectric constant at 65 GHz with ultimately high precision. This study aimed to establish an analytical algorithm to derive the hydration number from the measured frequency shift and to demonstrate the transition of hydration number upon thermal denaturation of human serum albumin. The determined hydration number in the native state drew a "global" hydration picture beyond the first solvation shell, with substantially reduced uncertainty of the hydration number (about ± 1 %). This allowed detection of a rapid increase in the hydration number at around 55°C during the heating process, excellently in phase with the irreversible rupture of the α-helical structure into solvent-exposed extended chains, whereas the hydration number did not trace the forward path in the subsequent cooling process. Our result indicates that weakening of water hydrogen bonds triggers unfolding of the protein structure first, followed by the changes in the number of hydration water as a consequence of thermal denaturation.

1. Introduction

Biochemical processes are inherently built on molecular fluctuations,[1-4] bathed in the flexible and dynamic hydrogen bond (HB) network of liquid water.[5] It is well known that at least a single layer of water molecules surrounding the protein surface (hydration level $h \approx 0.3$ g/g) yields the biological functionality of proteins, and dehydrated enzymes lose their activity.[6] In fact, the rigidity of the water HB networks correlates with the flexibility of the protein side-chains that are directly related to the protein activity.[6,7] However, even when hydrated, protein turns to a glassy-like state and as such its biological functions are suppressed below −70°C.[8] This fragile-to-strong dynamical transition arises from the interplay with hydration water in the vicinity of the protein surface, because reduced water mobility in turn inhibits protein side-chain motions.[9-14] At high temperatures, the second dynamical transition commonly referred to as the thermal denaturation, is observed.[15-20] Unlike the first transition at low temperatures, the second transition lets the protein to unfold its conformation irreversibly but how hydration water is engaged in this process is not yet fully understood.

Human serum albumin (HSA), a monomeric protein of 585 residues with a molecular weight of 66.5 kDa,[21] is one of the most well examined proteins in terms of its crystallographic structure and mechanisms of thermal denaturation.[22-28] It has three homologous domains I–III that assemble to form a heart-shaped three-dimensional structure,[22] and there is only a single Trp residue at position 214 in domain II and a single free Cys residue at position 34 in domain I.[29] Using the intrinsic Trp-214 and extrinsic label at Cys-34 as spectroscopic probes,[26,27] the unfolding process of HSA during thermal denaturation is found to consist of three phases. In the first phase (i), the temperature increase up to 50 ~ 55°C results in an initial expansion involving reversible separation of domains I and II. In the second phase, (ii) an intermediate structure in which domain II is irreversibly unfolded is formed by heating to <70°C, while in the third phase (iii), further heating eventually unfolds the closely packed

tertiary native structure of the protein.[26] Nevertheless, despite the detailed picture of HSA conformation during heating, the commitment of hydration water upon thermal denaturation is not well documented to date. This is because even though the contribution of hydration water in the functionality and dynamical transition of the protein has been primarily discussed in light of *mobility* of water hydrated to protein powder,[9-14,16-20] the *amount* of hydration water rarely comes up in the topic of debate. Furthermore, from a biological point of view, characterizing the hydration state in solution is more desirable than in powder samples, as motion of hydration water in solution is distinct from that around a hydrated powder.[30]

Since the complex dielectric functions $\tilde{\varepsilon}(\omega) = \varepsilon'(\omega) - i\varepsilon''(\omega)$ (permittivity ε' and dielectric loss ε'' as a function of angular frequency ω) below 100 GHz directly reflect bulk/hydration water dynamics, dielectric spectroscopy in the micro- and millimeter-wave regions provides quantitative information of the hydration state.[31-34] Yet, according to the large uncertainty of the hydration number (>5 %, typically corresponding to several dozen or hundred molecules), which is at the border of experimental accuracy, variations in the amount of hydration water during dynamical transition of protein have yet to be examined by dielectric spectroscopy. Alternatives to spectroscopic approaches are the narrow-band measurement systems that can uniquely measure $\tilde{\varepsilon}(\omega)$ with high precision, such as a cavity resonator[35] and metamaterial[36], which are more promising for finding tiny changes in the hydration state. Indeed, it was reported that the complex dielectric constant at 5.13 GHz estimated from the measured frequency shift of the cavity resonator significantly improved the uncertainty of the estimated hydration number.[37] From this perspective, a single-frequency resonator that is equipped with a high quality factor and is sensitive to the complex dielectric constant in the microwave or millimeter-wave regions can potentially open up the unexplored importance of hydration water to the protein functions.

Recently, the development of a novel complementary metal-oxide-semiconductor (CMOS) dielectric sensor that provides a change in the oscillation frequency as a result of the $\tilde{\varepsilon}(\omega)$ in the near-field has been advancing, and its operation frequency is now extended to millimeter or terahertz regions.[38-40] In particular, variable-control oscillator (VCO)-based CMOS that locks the oscillation at a certain frequency in a self-sustained manner has the advantage of measurement stability, circumventing fluctuation of an external source.[40] Mitsunaka *et al*. fabricated a silicon-based VCO-CMOS dielectric sensor consisting of arrayed 65 GHz LC resonators, and demonstrated ultimately stable oscillation (± 0.17 MHz, corresponding to 2.67 ppm).[38] Therefore, the ultimately precise and stable 65 GHz CMOS dielectric sensor has the potential to be the top candidate for sensing very minute changes in hydration water around the protein. Notwithstanding, they have yet to uniquely determine the complex dielectric constant $\tilde{\varepsilon} = \varepsilon' - i\varepsilon''$ using the sensor, since the measured LC oscillation frequency is dependent on two unknown parameters: permittivity ε' and dielectric loss ε''.

In this study, we aimed to quantitatively characterize the number of hydration water upon thermal denaturation of HSA, making full use of the high measurement precision of the state-of-art 65 GHz CMOS dielectric sensor. For this purpose, a broadband dielectric spectroscopy that measures $\tilde{\varepsilon}$ in a wide range of frequencies, was first carried out to interpret the underlying molecular dynamics observed at 65 GHz (section 3.1), and then, the relationship between the change in the oscillation frequency of the 65 GHz CMOS dielectric sensor and the amount of hydration water was established (section 3.3). In the meantime, temperature-dependent changes in the HSA secondary structure content were quantitatively examined with the aid of Fourier-transform infrared (FTIR) spectroscopy (section 3.2). Finally, the transition of the hydration number N_{hyd} during the thermal transition of HSA was investigated with high precision on the basis of a change in the oscillation frequency of the 65 GHz CMOS sensor (section 3.4).

2. Materials and methods

2.1 Sample preparation

HSA protein powder (>95 % purity) purchased from FUJIFILM Wako Pure Chemical Industry, Ltd. was used in this study without further purification. The native HSA aqueous solution at a concentration of 10 wt% (HSA molar concentration $C_{\mathrm{HSA}} = 1.5$ mM) was prepared by dissolving the powder sample into distilled water demineralized by >5 MΩ·cm. Density measurement was used to derive the stoichiometric molar concentration of water in the solution (C_{water}) and its molar ratio to that of pure water (ϕ_{water}).

2.2. Broadband dielectric spectroscopy

The complex dielectric function $\tilde{\varepsilon}(\omega)$ of pure water and the native 10 wt% HSA aqueous solution over a frequency range from 10 MHz to 12 THz was determined by impedance analyzer (IA), vector network analyzer (VNA), terahertz time-domain attenuated total reflection (THz TD-ATR), and far-infrared Fourier-transform attenuated total reflection (FIR FT-ATR) measurements. IA measurements between 10 MHz and 0.5 GHz were carried out with an RF LCR meter 4287A (Agilent Technologies) calibrated with open (air), short (a 0.5 mm-thick gold plate), and load (water).[41] A VNA system N5230 equipped with a dielectric probe kit 8507E and an ECal module N4693A (Agilent technologies) was used to measure the complex dielectric function in the frequency range from 0.5 to 50 GHz, after the three-point calibration procedure.[41] Frequencies over 50 GHz and 3 THz were measured by two THz TD-ATR spectroscopy systems, where a Dove prism made of a high-resistance monocrystalline silicon was employed. A TAS7500TS platform (ADVANTEST Corp.) connected to two low-temperature grown GaAs-based photoconductive (PC) antennas was used for the asynchronous optical sampling measurements in the lower frequencies (50 GHz ~ 1 THz),[42] and the higher-frequency counterpart from 1 to 3 THz was measured with a homebuilt system consisting of a femtosecond fiber laser (FemtoFErb780, TOPTICA Photonics AG) and two dipole PC antennas G10620-11 (Hamamatsu

Photonics KK). The complex dielectric function at the highest frequencies, 3 ~ 12 THz, was determined with the use of FIR FT-ATR measurements (FARIS-1s, JASCO Corp.), combined with the Kramers-Kronig transform.[42,43] In all of the above five experimental systems, the sample temperature was kept at 25°C with an accuracy of ± 0.1°C.

2.3 FTIR spectroscopy

The FTIR measurements were performed using an IRPrestige-21 spectrometer (Shimadzu) equipped with a MIRacle ATR accessory with a ZnSe crystal (PIKE Technologies). To avoid the systematic redshift of absorption bands inherent in ATR spectroscopy,[44] the Kramers-Kronig transform[43] was used to derive the absorption coefficient $\alpha(\nu)$ from the measured reflectance $R(\nu)$. Then, by subtracting the contribution of the solvent, the difference absorption spectrum $\delta\alpha(\nu)$ was obtained from 1350 to 1700 cm^{-1}, which is commonly used for secondary structure analysis.[45] The sample temperature was raised stepwise from 25°C to 75°C at 10°C intervals, and subsequently reversed to 25°C in the same manner, aiming to examine the temperature dependence of $\delta\alpha(\nu)$.

2.4 CMOS dielectric sensor consisting of 65 GHz LC resonators

The CMOS dielectric sensor embedding 65 GHz LC resonator structures, manufactured by Sharp Corporation, was used in this study.[38] As shown in Fig. 1, the metallic inducting wire and the gap of

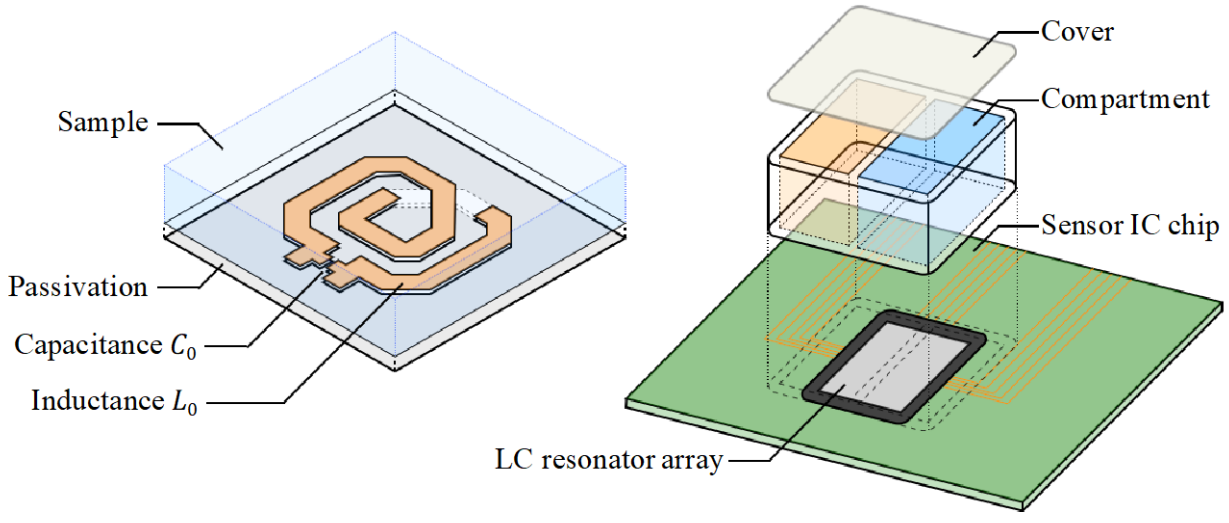

Fig. 1 Illustration of a 65 GHz LC-resonator element integrated in the CMOS sensor chip (left) and the measurement setup (right).

the structure are regarded as the inductance L_0 and the capacitance C_0 respectively; the LC resonator is protected by a passivation layer with a capacitance of C_1. Each resonator structure with a size of 0.008 mm^2 is arrayed as a 62 × 24 matrix in a zigzag manner, with a 40 μm spacing in the horizontal direction to minimize parasitic coupling with the adjacent elements. The gating time of each LC resonator was set at 200 μs with a delay time of 0.125 μs, allowing an effective frequency resolution of <0.33 MHz.

Because the electric field is localized within several dozens of micrometers from the chip surface,[38] each resonator feels the *effective* capacitance C_{eff} that includes the contribution from the passivation layer and the sample placed on it. Assuming a dielectric sample with a complex dielectric constant of $\tilde{\varepsilon}_2 = \varepsilon_2' - i\varepsilon_2''$ at 65 GHz resting upon the resonator, the LC oscillation frequency f is consequently described as

$$f = \frac{1}{2\pi\sqrt{L_0 C_{\text{eff}}}} = \left[2\pi\sqrt{L_0\left\{C_0 + C_1\frac{C_1C_2 + {C_2}^2 + {G_2}^2}{(C_1 + C_2)^2 + {G_2}^2}\right\}}\right]^{-1} \quad (1)$$

where, $C_2 = C\varepsilon_2'$ and $G_2 = C\varepsilon_2''$ (C: constant) are the capacitance and conductance of the sample,[38] respectively. Eqn. (1) indicates that f undergoes a low-frequency shift in the presence of the sample, demonstrating the potential of this sensor as a quantitative index to estimate the complex dielectric constant $\tilde{\varepsilon}_2$ of the sample at 65 GHz. To relate directly the resonant frequency f with $\tilde{\varepsilon}_2$, the temperature dependence of air and pure water was recorded over $20 \leqq T \leqq 80$°C to determine the instrumental constants L_0, C_0, C_1 and C, using a nonlinear least-square fitting procedure, as a calibration measurement (see the ESI S1 for details).

After the calibration, a 2-well silicone compartment with a maximum volume capacity of 70 μL was directly adhered to the LC resonant array area (~ 3 mm square) of the sensor chip through a water-impermeable adhesive, in order to evenly divide it into two measurement sections. By sealing the silicon compartment with a cover glass, undesirable sample evaporation was avoided. The rear

surface of the sensor chip was attached to a Peltier temperature control unit to vary the sample temperature, consistently between the two compartments. Following a background measurement in air, the respective sections of the well compartment were filled with pure water and the 10 wt% HSA solution, and then the frequency shift Δf defined by Eqn. (2) was determined:

$$\Delta f = f_{\mathrm{BKG}} - f_{\mathrm{SAM}} \tag{2}$$

where f_{BKG} and f_{SAM} are the oscillation frequencies of the background and sample measurements, respectively. As for the sample measurements, the time-lapse data acquisition of f_{SAM} at regular intervals was launched under the (i) "temporal" heat treatment and (ii) "step-by-step" heat treatment. The former involved a rectangular-like temperature change 25°C → ~70°C (for 15 min) → 25°C, so as to compare the frequency shift Δf at $T =$ 25°C before and after the heating treatment. In the latter experiment, the sample temperature was raised from 25°C to ~ 80°C, at nearly regular intervals, in a stepwise manner and then similarly reversed to 25°C, with the aim of examining the temperature dependence of Δf. In common to these two experiments, variation in the measured oscillation frequency f was locked within ± 1 MHz during the entire measurement, ensuring the long-term stability of our system (see the ESI S2).

3. Results and discussion

3.1 Identification of the molecular dynamics at 65 GHz

The broadband complex dielectric spectra $\tilde{\varepsilon}(\omega)$, from 10 MHz to 12 THz, of pure water and the native 10 wt% HSA aqueous solution at $T =$ 25°C are shown in Fig. 2(a). With regard to pure water, a huge dispersion around 20 GHz (hereafter called γ1 mode) is derived from the collective reorientational relaxation of bulk water, while an additional relaxation mode (γ2) exists in the sub-THz region with an intensity approximately 50 times smaller than the γ1 relaxation.[42,46] Beyond 1 THz, several intermolecular vibration modes of water, such as the intermolecular bending (B) centered around 1.5

THz, the intermolecular stretching (S) around 5 THz and the libration (L) around 18 THz, have an increasing impact.[42] The fact that the real part $\varepsilon'(\omega)$ below 1 GHz converges to the static permittivity (78.38) indicates that no other water dynamics are responsible for the dielectric responses in the lower frequencies, except for a faint electric conductivity tail observed in the dielectric loss spectrum $\varepsilon''(\omega)$. For the 10 wt% HSA aqueous solution, the dielectric loss $\varepsilon''(\omega)$ exhibits a slightly smaller main relaxation relative to pure water, reflecting a decreased molar concentration of bulk water. The permittivity spectrum $\varepsilon'(\omega)$ with dispersion below 1 GHz is indicative of the presence of other mode(s) that is dynamically slower than the bulk water relaxations, although it is masked by a considerably large electric conductivity in $\varepsilon''(\omega)$. Certainly, some of the vibration density of states of protein solute are infrared-active,[47,48] but they are considered negligible in our case because their contribution is 2 orders smaller than that of the water modes.[49]

In order to reveal the underlying components behind the spectra, the complex dielectric function $\tilde{\varepsilon}(\omega)$ of the HSA solution was fitted with Eqn. (3), following previous studies:[31-34,42]

$$\begin{aligned}\tilde{\varepsilon}(\omega) - \frac{\sigma}{i\omega\varepsilon_0} &= \tilde{\chi}_\beta(\omega) + \tilde{\chi}_{\delta 1}(\omega) + \tilde{\chi}_{\delta 2}(\omega) + \tilde{\chi}_{\gamma 1}(\omega) + \tilde{\chi}_{\gamma 2}(\omega) + \sum_{\mathrm{v=B,S,L}} \tilde{\chi}_\mathrm{v}(\omega) + \varepsilon_\infty \\ &= \frac{\Delta\varepsilon_\beta}{1+i\omega\tau_\beta} + \frac{\Delta\varepsilon_{\delta 1}}{1+i\omega\tau_{\delta 1}} + \frac{\Delta\varepsilon_{\delta 2}}{1+i\omega\tau_{\delta 2}} + \frac{\Delta\varepsilon_{\gamma 1}}{1+i\omega\tau_{\gamma 1}} + \frac{\Delta\varepsilon_{\gamma 2}}{1+i\omega\tau_{\gamma 2}} \\ &\quad + \sum_{\mathrm{v=B,S,L}} \frac{\Delta\varepsilon_\mathrm{v}{\omega_\mathrm{v}}^2}{{\omega_\mathrm{v}}^2 - \omega^2 + i\omega\Gamma_\mathrm{v}} + \varepsilon_\infty \end{aligned} \quad (3)$$

where, $\tilde{\chi}_\beta(\omega)$, $\tilde{\chi}_\delta(\omega)$ and $\tilde{\chi}_\gamma(\omega)$ are the Debye-type complex susceptibilities (relaxation strength $\Delta\varepsilon$ and relaxation time τ) of β- (protein), δ- (mainly hydration water), and γ- (bulk water) relaxation processes, respectively, and $\tilde{\chi}_\mathrm{v}(\omega)$ is the damped harmonic oscillator model ($\Delta\varepsilon_\mathrm{v}$: vibration strength, $\omega_\mathrm{v}/2\pi$: resonant frequency, and $\Gamma_\mathrm{v}/2\pi$: damping constant) representing the intermolecular vibration modes of water (v = B, S, L), and ε_∞ is the high-frequency limit of the permittivity. The term $\sigma/i\omega\varepsilon_0$ (where σ is the electric conductivity and ε_0 is the permittivity of vacuum) corresponds to

the loss by conductivity. As shown in Fig. 2(b), the conductivity-free complex dielectric spectrum $\tilde{\varepsilon}(\omega) - \sigma/i\omega\varepsilon_0$ of the native 10 wt% HSA solution was well reproduced by Eqn. (3), and the obtained best-fitted parameters are consistent with previously reported values.[34,35,42]

Figs. 2(a) and (b) clearly indicate that the total contribution of the conductivity term ($\sigma/i\omega\varepsilon_0$) and the non-bulk water relaxation modes ($\tilde{\chi}_\beta + \tilde{\chi}_{\delta 1} + \tilde{\chi}_{\delta 2}$) to the complex dielectric function $\tilde{\varepsilon}(\omega)$ above 50 GHz is extremely small. However, beyond 300 GHz, the growing contribution of the intermolecular vibration modes of water ($\sum \tilde{\chi}_v$) makes it difficult to separate the bulk/hydration water dynamics, as their line-shapes are hardly discerned.[49-51] According to these findings, we emphasize here that the dielectric constant $\tilde{\varepsilon}$ in the 65 GHz region observes *selectively* the bulk water relaxation dynamics without interference from the protein solute and hydration water modes. Therefore, when limited to this frequency region, Eqn. (3) used to fit the complex dielectric function $\tilde{\varepsilon}(\omega)$ of the 10 wt% HSA aqueous solution can be more simply approximated as the following equation.

$$\tilde{\varepsilon}(\omega) \approx \tilde{\chi}_{\gamma 1}(\omega) + \tilde{\chi}_{\gamma 2}(\omega) + \varepsilon_\infty$$

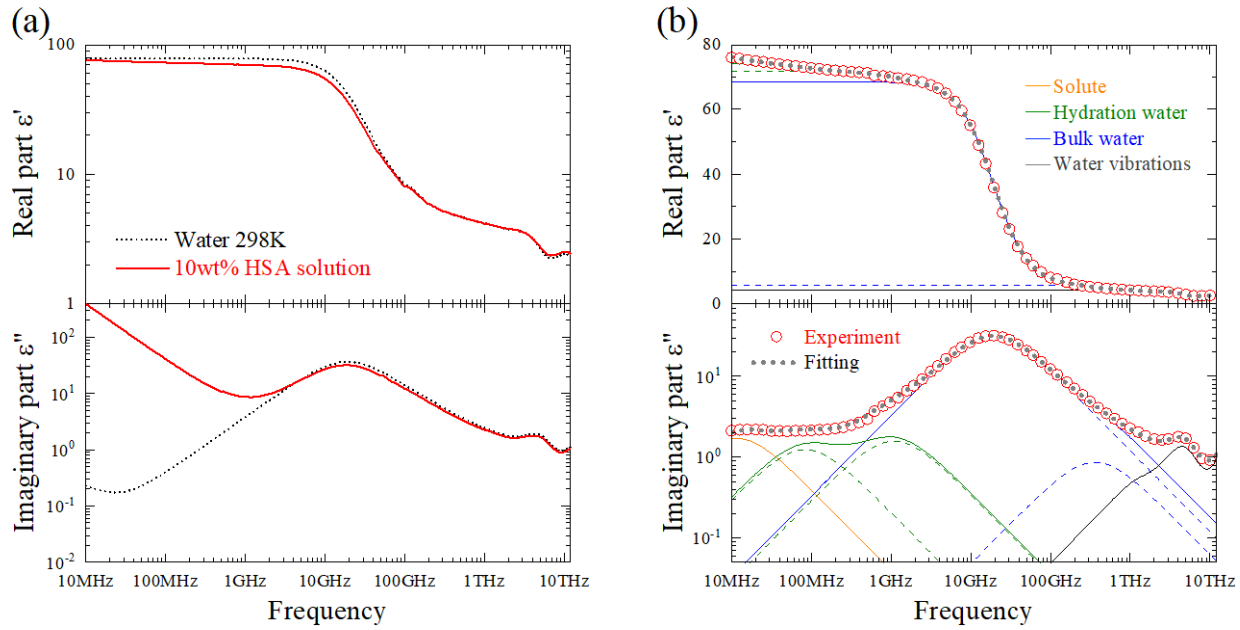

Fig. 2 (a) Complex dielectric spectra of pure water and the native 10% HSA aqueous solution at 25°C over 10 MHz and 12 THz (upper panel: permittivity $\varepsilon'(\omega)$, lower panel: dielectric loss $\varepsilon"(\omega)$). The broken lines depict the electric conductivity terms $\sigma/i\omega\varepsilon_0$ (see text). (b) Conductivity-free complex dielectric spectrum of the 10 wt% HSA aqueous solution and its constituent subcomponents described by Eqn. (3).

$$= \frac{\Delta\varepsilon_{\gamma 1}}{1 + i\omega\tau_{\gamma 1}} + \frac{\Delta\varepsilon_{\gamma 2}}{1 + i\omega\tau_{\gamma 2}} + \varepsilon_{\infty} \quad (4)$$

It should be noted that this approximation is the case for a solute molecule with as large molecular weight as a protein, but not for small osmolyte molecules such as saccharides, amino acids, and urea (see the ESI S3).

With regard to the γ1-process, our spectrum decomposition analysis provided $\Delta\varepsilon_{\gamma 1} = 62.84 \pm 0.18$ for the native 10 wt% HSA solution at 25°C. The smaller relaxation strength compared to pure water ($\Delta\varepsilon_{\gamma 1}^{\mathrm{w}} = 72.70 \pm 0.18$) is attributed to the decreased amount of bulk water, since the relaxation strength $\Delta\varepsilon$ is proportional to the number density of the dipole.[49-51] Then, the ratio of bulk water in the solution to that in pure water, ϕ_{bulk}, is calculated using Eqn. (5).[32,33]

$$\phi_{\mathrm{bulk}} = \frac{\Delta\varepsilon_{\gamma 1}}{\Delta\varepsilon_{\gamma 1}^{\mathrm{w}}} \quad (5)$$

The obtained bulk water fraction ($\phi_{\mathrm{bulk}} = 0.864 \pm 0.03$) is significantly smaller than the stoichiometric water ratio ($\phi_{\mathrm{water}} = 0.915$) determined by our density measurement, suggesting that a subset of water molecules in the solution turns to hydration water in the presence of protein solute. Defining hydration water as all water molecules that no longer contribute to the bulk water relaxation process, the number of hydration water per solute (hydration number N_{hyd}) is determined by

$$N_{\mathrm{hyd}} = \frac{C_{\mathrm{water}} - C_{\mathrm{bulk}}}{C_{\mathrm{HSA}}} \quad (6)$$

where $C_{\mathrm{bulk}} = \phi_{\mathrm{bulk}} \cdot \rho_{\mathrm{w}}/M_{\mathrm{w}}$ (ρ_{w} and M_{w}: density and molecular weight of pure water, respectively) is the bulk water concentration in the 10 wt% HSA solution.[32,33] According to Eqn. (6), our data yielded $N_{\mathrm{hyd}} = 1893 \pm 123$ (corresponding to 0.514 ± 0.033 g/g solute), which is in excellent agreement with a previous dielectric measurement finding $N_{\mathrm{hyd}} = 1840$.[37] From a geometrical point of view, however, the number of water molecules required to form a complete first hydration layer around HSA is approximately 1070 (~ 0.3 g/g),[37] and small-angle scattering experiments revealed that the number of *tightly* bound water molecules surrounding an HSA solute is approximately

1100.[52,53] Since Eqns. (5) and (6) define any water molecules with distinctly retarded reorientation dynamics as hydration water, *loosely* constrained water beyond the first hydration layer and *tightly* bound water are both regarded as hydration water. Seemingly, analysis of the δ relaxation processes that observe hydration water dynamics draws a more straightforward and valuable picture about the hydration state, rather than our indirect strategy. From a practical point of view, however, the origins of the δ-processes are so complicated that it is much more difficult to quantitatively interrelate them with the hydration state.[54]

3.2 Estimation of the secondary structure using FTIR spectroscopy

Since the C=O bond length and energy are modulated by HB and transition dipole-dipole coupling but is hardly affected by the nature of the side-chains (see the ESI S4),[45,55] the peak wavenumber inhomogeneity of carbonyl stretching vibration (so-called amide I; 1600 ~ 1700 cm^{-1}) provides information about the secondary structure. The amide II (1500 ~ 1600 cm^{-1}) and III (1200 ~ 1400 cm^{-1}) bands are also subject to backbone conformation, although their correlation with the protein secondary structure is less straightforward than that of amide I.[45]

In our stepwise temperature changes, the forward (heating) process from 25°C to 75°C causes markedly reduced absorption $\delta\alpha(\nu)$ over 1350 cm^{-1} and 1700 cm^{-1}, as shown in the upper panel of Fig. 3(a) and Fig. S4 in the ESI. In the recovery (cooling) process down to 25°C, however, $\delta\alpha(\nu)$ is much less sensitive to temperature, implying little refolding of the HSA secondary structure. As each secondary structure element gives rise to inherent amide I sub-band at slightly different wavenumbers,[56] the modified amide I band shape is interpreted as variation in the secondary structure contents due to denaturation.[57-59] Computing second derivative spectrum is one of the most common numerical approaches to separate highly overlapping components without an arbitrary choice of deconvolution parameters.[59] As shown in the lower panel of Fig. 3(a), the calculated second derivative

$d^2\delta\alpha(\nu)/d\nu^2$ obviously exhibits distinct signatures upon thermal denaturation: the native HSA (forward 25°C) is characterized as three relatively sharp components, while after thermal denaturation (75°C and recovered 25°C) only broad and weak bands are recognizable. In the native state, the most intense sub-band at 1654 cm^{-1} and the weak component at 1680 cm^{-1} can be safely assigned to the α-

helix and β-turn components, respectively.[56-59] The low-wavenumber sub-band around 1632 cm^{-1} has long been considered to originate from β-sheets[59] but recently it was pointed out that this assignment likely overestimates the β-sheet content of globular proteins such as HSA.[60] Meanwhile, the amide I wavenumber of α-helices is known to downshift by ~ 20 cm^{-1} upon hydration when the backbone

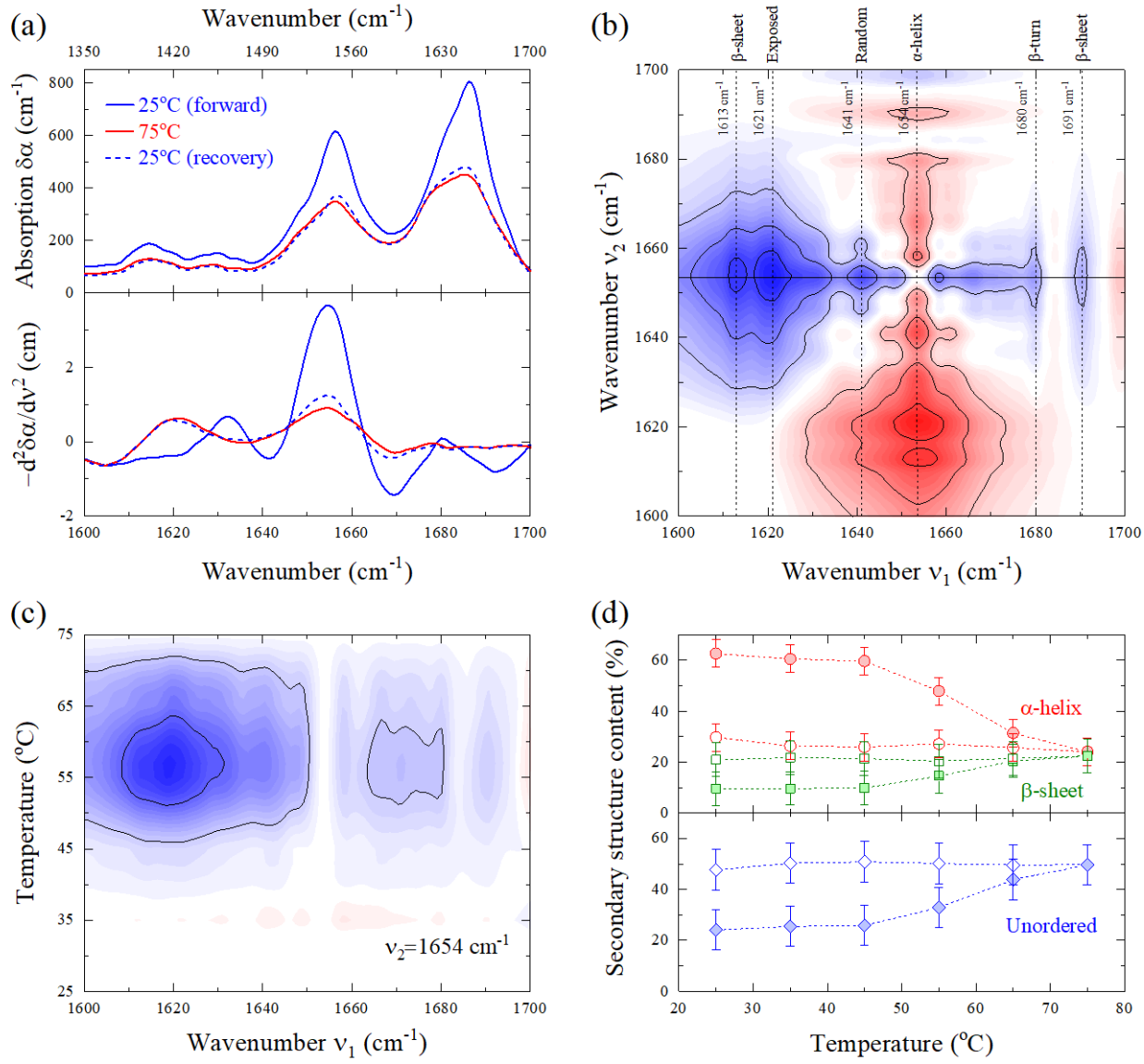

Fig. 3 (a) Difference absorption spectrum $\delta\alpha(\nu)$ over 1350 and 1700 cm^{-1} and its second derivative $d^2\delta\alpha(\nu)/d\nu^2$ in the amide I region (1600 $\leqq \nu \leqq$ 1700 cm^{-1}; note that the second derivative is displayed by reversing the positive and negative signals). (b) Generalized 2D asynchronous correlation contour $\Psi(\nu_1, \nu_2)$ in the amide I region. The red and blue areas correspond to positive and negative correlations, respectively. The horizontal black line represents $\nu_2 =$ 1654 cm^{-1}. (c) Moving-window asynchronous 2D correlation contour $\Psi(\nu_1, T)$ sliced at $\nu_2 =$ 1654 cm^{-1}. Positive and negative correlations are displayed in the same color as (b). (d) Estimated content of α-helices, β-sheets, and unordered (including both the random coil and extended) structures. The β-turn structure (~ 3.6 %, independent of temperature) is not depicted. The forward and recovery processes at 25 °C are described as closed and open symbols, respectively.

C=O group forms a bifurcated HB to a water molecule in the out-of-plane direction.[61-63] For this reason, in the case of helical-rich HSA,[22-24] it is supposed that both β-sheets and hydrated α-helix are the main factor giving rise to the 1632 cm^{-1} sub-band.

Upon heating to 75°C and subsequent recovery to 25°C, the 1632 cm^{-1} and 1654 cm^{-1} sub-bands are substantially reduced, while a new sub-band is alternatively evolved around 1620 cm^{-1}, suggesting replacement of α-helices with other secondary structures due to irreversible unfolding. Nevertheless, the interpretation of this denaturation-derived band at ~ 1620 cm^{-1} is complicated by the two over-lapped components close in peak position.[64,65] In the present study, this problem was resolved by applying the generalized two-dimensional (2D) correlation analysis to the measured $\delta\alpha(\nu)$ for spectral resolution enhancement, using temperature T as a disturbing variable.[66] The 2DShige© software developed by Shigeaki Morita (Kwansei-Gakuin University, 2004-2005), was used to calculate the synchronous Φ and asynchronous Ψ correlation plots that visualize, respectively, in-phase and out-of-phase absorption variations with temperature. The obtained asynchronous correlation $\Psi(\nu_1, \nu_2)$ presented in Fig. 3(b) successfully discloses hidden sub-bands behind the complex amide I spectrum, in contrast to the limited information provided by the synchronous one (Fig. S5 of the ESI). When focusing on the correlation with the α-helix band at $\nu_2 =$ 1654 cm^{-1}, the denaturation-derived sub-bands were identified at $\nu_1 =$ 1613 cm^{-1}, 1621 cm^{-1}, 1641 cm^{-1}, and 1691 cm^{-1}, apart from the afore-mentioned β-turn at 1680 cm^{-1} (a weak correlation at 1658 cm^{-1} may be an additional α-helix peak[59]). The *negative* correlations with $\nu_2 =$ 1654 cm^{-1} indicate that the evolution of these bands is subse-quent to the loss of α-helices.[66] Consistent with earlier studies on thermally denatured albumin,[64,65] our generalized 2D correlation analysis exposes the overlapping two sub-bands at 1613 cm^{-1} and 1621 cm^{-1} merged into the broad ~ 1620 cm^{-1} component in the second derivative spectra. In light of the characteristic amide I wavenumber examined so far, the lowest (1613 cm^{-1}) and highest (1691 cm^{-1}) wavenumber components can be reasonably attributed to the intermolecular and intramolecular β-

sheets, respectively. The most possible assignment for the 1641 cm^{-1} component is the random or irregular structure[45] (though a possible contribution of the H-O-H bending of hydration water cannot be eliminated)[67]. Overall, this observation is consistent with the widely accepted picture that thermal denaturation increases the content of β-sheet and random coil structures at the expense of α-helix.[59] The strongest correlation observed at $\nu_1 = 1621$ cm^{-1} is generally believed to originate from extended β-strands or β-sheets,[55,59] but several authors raised a concern about this assignment since it inevitably overestimates the β-sheet content of globular proteins.[60,68] A clue to settle this controversy is found in previous FTIR spectroscopy studies of temperature-responsive polymers such as poly(*N*-isopropylacrylamide), which revealed that stretching vibration of carbonyl group forming an intermolecular HB with water (C=O … H_2O) absorbs around 1620 cm^{-1}.[69-71] Corroborated by the simulated amide I spectrum of water-exposed short peptide,[72] we reached the conclusion that the 1621 cm^{-1} sub-band that emerged in the thermally denatured state is more likely related with the extended side-chain forming a HB with water, rather than the β-sheet.

We further examined the denaturation-derived amide I sub-bands in terms of their temperature dependence with the aid of a moving-window 2D correlation analysis that allows us to obtain the spectral correlation with ν_2 on a plane between the wavenumber ν_1 and temperature T axes.[73] Fig. 3(c) shows the moving-window asynchronous contour $\Psi(\nu_1, T)$ correlated with the α-helix component ($\nu_2 = 1654$ cm^{-1}). Despite little correlation below 50°C, $\Psi(\nu_1, T)$ exhibits strong negative correlations above the unfolding temperature of HSA (~ 55°C),[26] especially in the intermolecular β-sheet ($\nu_1 = 1613$ cm^{-1}) and extended chain (1621 cm^{-1}) sub-band regimes. Considering that *negative* asynchronous correlation $\Psi(\nu_1, T)$ represents a steep and non-linear absorption change upon temperature increase, our results show that at approximately 55°C α-helices in the native state are rapidly replaced by denatured structures.

On the basis of the above relationship between the amide band spectra and the secondary structures

of the protein, we then estimated quantitatively the contents of the secondary structure elements using a mathematical model proposed by Goormaghtigh and his co-workers.[68] The evaluated contents at 25°C before denaturation (62.6 % for α-helix, 9.7 % for β-sheet, 3.6 % for β-turn, and 24.1 % for unordered structure) presented in Fig. 3(d) are in good agreement with the circular dichroism (CD) spectroscopy,[28,74-77] eliminating thus the systematic overestimation of the β-sheet content pertaining to curve fitting of the amide I spectrum. Note that the "unordered" category involves structures that do not have a regular HB pattern, such as water-exposed chain/loop structures and random coils. Although the native secondary structure is maintained at pre-denaturation temperatures, a monotonous decrease in the fractional α-helix content starts from ~ 50°C and the disrupted helices do not show complete recovery upon cooling because they are reorganized into β-sheets and unordered structures in an irreversible manner. Remarkably, the unordered structures exhibit a larger increase than the β-sheets, and their final content (~ 50 %) surpasses that of α-helices at 75°C and is kept mostly constant during the whole subsequent recovery. Based on the strongest correlation of the $\nu_2 =$ 1654 cm^{-1} sub-band with the $\nu_1 =$ 1621 cm^{-1} found in this study (Fig. 3(b)), it is considered that the native secondary structure of HSA rich in α-helices was mainly transformed into extended structures in the thermally denatured state, with a relatively small content of α-helix, intermolecular β-sheet, and random coil conformers.

3.3 Assessment of the bulk water fraction ϕ_{bulk} from Δf

Fig. 4(a) shows the oscillation frequency f of air and water, and the corresponding frequency shift Δf as a function of temperature. It was found that the oscillation frequency of pure water $f_{\mathrm{SAM}}(T)$ undergoes a noticeable downshift with increasing temperature, which results in a monotonous increase in $\Delta f(T)$. This variance can be primarily explained by the temperature dependence of the complex dielectric constant $\tilde{\varepsilon}$ at 65 GHz. Nevertheless, the oscillation frequency of air, whose dielectric constant is fixed ($\tilde{\varepsilon} = 1$) independently of T, also changes with temperature albeit slightly,

implying temperature-dependent instrumental constants $L_0(T)$, $C_0(T)$ and $C_1(T)$ (see the ESI S1 for details). As illustrated in Fig. 4(b), the contour plot of the frequency shift $\Delta f(\varepsilon_2', \varepsilon_2'')$ of pure water at 25°C calculated on the basis of Eqns. (1) and (2) reveals a pronounced high-frequency shift of Δf upon increasing ε_2' or ε_2''. From this plot, it is also obvious that the frequency shift Δf can be uniquely estimated from the complex dielectric constant $\tilde{\varepsilon}_2 = \varepsilon_2' - i\varepsilon_2''$ at 65 GHz, but not *vice versa*. In other words, a single solution of $(\varepsilon_2', \varepsilon_2'')$ at 65 GHz cannot be *uniquely* derived from the frequency shift Δf because numerous possible $(\varepsilon_2', \varepsilon_2'')$ pairs have the same Δf value. Therefore, an additional constraint is required to characterize the hydration state from the measured Δf.

A clue to settle this issue is offered by our dielectric spectroscopy finding in section 3.1 that the dielectric responses at 65 GHz can be approximated by Eqn. (4). Previous dielectric studies have shown that the relaxation times $\tau_{\gamma 1}$ and $\tau_{\gamma 2}$ hardly depend on protein concentration and conformations,[33,49,78] and hence they can be reasonably assumed identical to those of pure water at the same temperature. Furthermore, assuming that the high-frequency permittivity ε_∞ linearly changes from 4.2 (pure water)[42] to 2.7 (HSA crystalline)[49], the locus of $(\varepsilon_2', \varepsilon_2'')$ pairs at 65 GHz depending on the

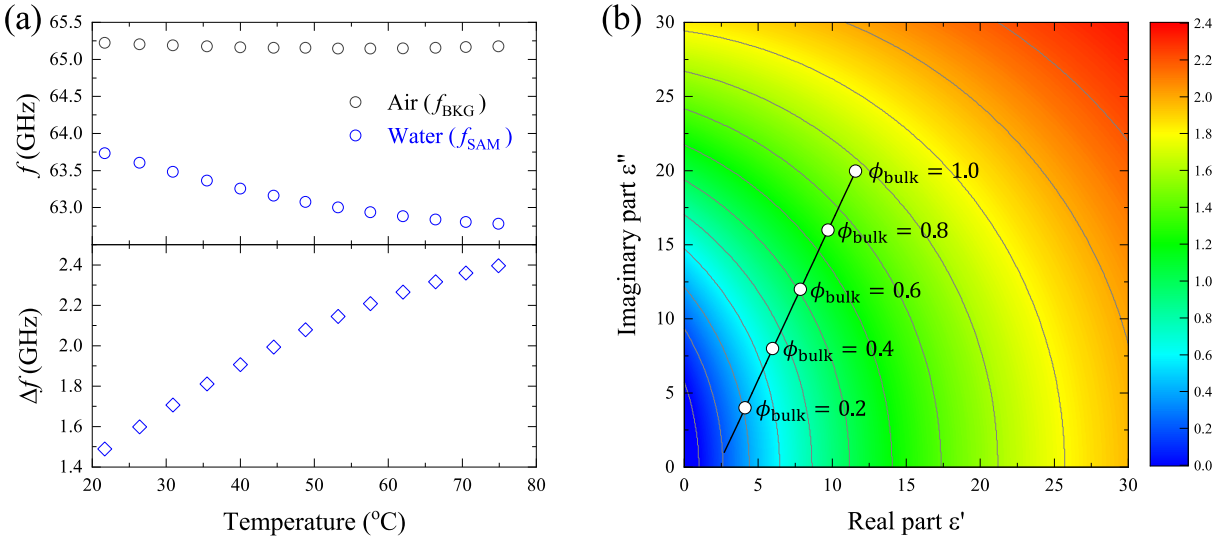

Fig. 4 (a) Oscillation frequencies f_{BKG}(air) and f_{SAM}(pure water) and the frequency shift Δf as a function of temperature. (b) Contour plot of the frequency shift $\Delta f(\varepsilon_2', \varepsilon_2'')$ for pure water at 25°C. The black solid line represents the locus of the complex dielectric constant at 65 GHz as a function of the bulk water fraction ϕ_{bulk} defined by Eqn. (5). The empty circles correspond to the representative values (ϕ_{bulk} = 0.2~1.0 at 0.2 intervals).

bulk water fraction ϕ_{bulk} draws the black solid line in Fig. 4(b). It is clearly seen that the estimated $(\varepsilon_2', \varepsilon_2'')$ coordinate moves from the upper right to the lower left at nearly regular intervals, as ϕ_{bulk} changes from 100 % (pure water) to the waterless situation. More importantly, the depicted locus lies in the direction orthogonal to the contour lines of Δf, leading to a one-on-one correspondence of ϕ_{bulk} with Δf. This way, the bulk water fraction ϕ_{bulk} can be uniquely determined from the measured frequency shift Δf, and eventually, the hydration number N_{hyd} can be successfully derived with the aid of Eqn. (6).

3.4 Characterization of the hydration state upon thermal denaturation

Simultaneous measurement of pure water and the 10 wt% HSA aqueous solution allowed us to record the time dependent Δf upon "temporal" heating treatment, where the sample temperature rapidly increased from $T =$ 25°C to 70°C at $t =$ 2.0 h and then recovered to $T =$ 25°C after an elapse of 15 minutes. The results in Fig. 5(a) show first that the frequency shift Δf of pure water is greater than that of the 10 wt% HSA solution at any time, reflecting the larger complex dielectric constant for pure water at 65 GHz. Second, rapid upshifts of Δf at $t =$ 2.0 h are attributed to the rectangular-like temperature variation (25°C→70°C→25°C), since the frequency shift Δf varies

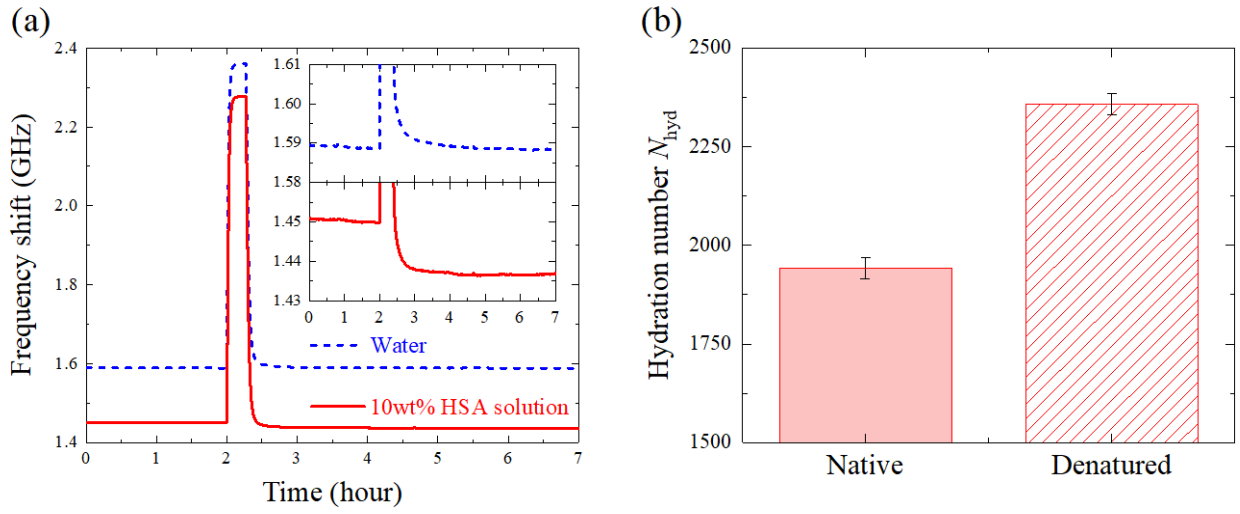

Fig. 5 (a) Time-dependent changes in the frequency shift $\Delta f(t)$ of pure water and the 10 wt% HSA aqueous solution. Heating at $T =$ 70°C was temporally treated for 15 min starting at $t =$ 2.0 h. The insets show enlarged views at approximately $T =$ 25°C. (b) Hydration number N_{hvd} of native and denatured HSA molecules at 25°C. The error bars correspond to the standard errors of three replicate experiments.

sensitively with temperature, as confirmed in Fig. 4(a). The enlarged views displayed in the insets of Fig. 5(a) make more obvious the differences between before and after temporal heating. On one hand, the frequency shift Δf of pure water exhibits a back-and-fourth behavior, ensuring temperature consistency and long-term stability. On the other hand, the frequency shift Δf of the 10 wt% HSA aqueous solution is not reversed; consequently, the Δf difference between pure water and the HSA solution before heating (138.7 ± 0.9 MHz) is widened to 151.7 ± 0.9 MHz after cooling (note that long-term variation of our system is less than ± 1.6 MHz; see the ESI S2).

As the β- (protein) and δ- (hydration water) relaxation processes have negligible influence on the complex dielectric constant at 65 GHz even in the thermally denatured state due to their long relaxation time,[79] the smaller value of Δf after recovery definitely represents decreased molar fraction of bulk water attributed to thermal denaturation. To express more quantitatively the hydration state of HSA, the hydration number N_{hyd} at 25°C was determined by means of Eqn. (6) via estimating the bulk water fraction ϕ_{bulk} from Δf. As shown in Fig. 5(b), the obtained $N_{\mathrm{hyd}} = 1939 \pm 27$ in the native state agrees well with our dielectric spectroscopy result ($N_{\mathrm{hyd}} = 1893 \pm 123$), verifying our measurement and analysis. It should be emphasized here that the derived uncertainty of N_{hyd} is only about one-fifth of that determined by dielectric spectroscopy, owing to the highly accurate and stable oscillation at 65 GHz. Indeed, the uncertainty of the measured Δf (± 0.4 MHz) corresponds to only ± 0.024 and ± 0.012 for permittivity ε' and dielectric loss ε'', respectively. These values are significantly smaller than the standard error of our dielectric spectroscopy measurement at 65 GHz (greater than ± 0.08 for ε' and ± 0.04 for ε''; signal-to-noise ratio of $>10^4$). The above argument leads to the conclusion that our CMOS dielectric sensor derives a N_{hyd} value consistent with that of dielectric spectroscopy, but its precision is significantly improved due to the highly stable oscillation of the LC resonators.

As mentioned in section 3.1, the determined N_{hyd} for native HSA is substantially greater than the

number of water molecules that are densely packed in the first solvation shell (~ 1100)[52,53] with an average thickness of ~ 3 Å,[80,81] where water structure and dynamics are profoundly distinct from the bulk.[82] Taking advantage of a linear relationship between the hydration shell thickness and the hydration number reported by molecular dynamics simulation of a globular protein,[82] we roughly estimated the thickness of the hydration shell as ~ 3.85 Å in the case of native HSA. In the present analysis, we regarded hydration water as those molecules no longer contributing to the collective relaxation process of bulk water $\tilde{\chi}_{\gamma 1}$.[84,85] Since the structure and dynamics of hydration water at the very vicinity of the protein surface are driven by the local interactions with the surface residues and geometrical constraints,[86] their correlation with bulk water dynamics fades away. Restoring the bulk water dynamics occurs at long distance from the protein surface into the bulk due to global dynamical collectivity,[87] therefore, a subset of water molecules beyond the first solvation layer is dynamically distinguished from the $\tilde{\chi}_{\gamma 1}$ process and as such is identified as hydration water in our definition.[88]

As presented in Fig. 5(b), the hydration number N_{hyd} was found to increase by ~ 20 % after temporal heating. Even though only a few studies so far have focused in characterizing the *amount* of hydration water upon thermal denaturation of proteins, our result is consistent with an exceptional work by Hédoux *et al.*, who measured the OH stretching Raman spectrum of hydrogenated lysozyme in D_2O solvent and found an increased hydration number in the denatured state.[89] Nevertheless, their hydration number for native lysozyme (158 ± 8), corresponding to $h \approx 0.2$ g/g, likely observes only a part of the first hydration layer, since such tightly bound water molecules that protein-solvent isotopic exchanges can easily occur are regarded as hydration water in their definition. Hence, our work is the first to describe the whole picture of the hydration number N_{hyd} upon thermal denaturation. From a thermodynamic point of view, protein folding into native globular conformation is driven by hydration entropy, whereas upon unfolding, the large energy loss by the intramolecular interactions

in a protein is largely compensated for by a corresponding gain from hydration enthalpy.[90,91] Hydration water with restricted dynamics having smaller entropy than bulk, lesser N_{hyd} in the native state agrees well with a concept that a protein folds into its native structure to maximize the entropy of solvent water.[91] Furthermore, our study shows that the large gain from hydration enthalpy upon unfolding results from the growth in N_{hyd} at a microscopic level.

To explore the underlying mechanism regarding the hydration state in more detail, we also examined the temperature dependence of Δf when the sample's equilibrium temperature was varied in a stepwise manner (the "step-by-step" experiment). As presented in Fig. 6(a), $\Delta f(T)$ of pure water undergoes a monotonous upshift with temperature, and the reversed route is perfectly followed when cooling. In contrast, the 10 wt% HSA solution heated up to ~ 80°C obviously exhibits hysteresis behavior, showing smaller $\Delta f(T)$ in the recovery process (open circles) compared with that in the forward (closed circles). The measured frequency shifts $\Delta f(T)$ of pure water and the HSA solution at each temperature were then converted to the bulk water ratio, $\phi_{\mathrm{bulk}}(T) = \Delta\varepsilon_{\gamma 1}(T)/\Delta\varepsilon_{\gamma 1}^{\mathrm{w}}(T)$, and finally, the hydration number $N_{\mathrm{hyd}}(T)$ was determined. As summarized in Fig. 6(b), N_{hyd} monotonously increases as raising temperature with a huge jump at around 55°C where the helical-rich secondary structure of HSA starts to fall apart. The rapid rise in N_{hyd} perfectly in phase with replacement of α-helices with water-exposed extended chains (Fig. 3(d)) clearly declares that hydration to exposed backbone and side-chains is responsible for the increased N_{hyd} when a globular HSA moves to a thermally denatured form. In other words, the increased *amount* of hydration water should be the result of protein unfolding. Meanwhile, Mallamace and his co-workers experimentally revealed that subtle enhancement of hydration water *mobility* due to weakened HBs at high temperatures lets protein to unfold,[17-20,92,93] due to conformational flexibility of backbone and side-chains.[94-96] These complementary evidences lead to the conclusion that the loosened hydration shell upon heating triggers thermal denaturation by increasing conformational entropy of protein, and the hydration number

N_{hyd} is increased as a consequence. Nevertheless, the highly stable hydration shell consisting of a minimum quantity of water molecules around native protein is disappeared and becomes more unstable upon thermal denaturation, owing to less restricted exposed backbone and side-chains.[97]

Since our FTIR spectroscopy analysis showed that each secondary structure content linearly varies up to 75°C, an inflection point around 62°C cannot be explained the secondary structure alone: reduction in the slope above $T \approx$ 62°C can be rationalized by partial release of hydration water caused by thermally accelerated backbone and side-chain motions that inhibits surrounding water to form stable HBs,[94-96] and aggregation that results in the exclusion of water molecules from the protein surface. The slight increase in N_{hyd} below 55°C may have its roots in the overall expansion involving growth of solvent-accessible surface area (SASA) while keeping the native secondary structures.[26] With regard to the recovery process from ~ 80°C to 25°C, the downward trend in N_{hyd} via a different path from the heating process is undoubtedly ascribed to *irreversible* thermal denaturation. This is not the case with reversible unfolding by heating up to 45°C, where the hydration number traces its forward path, as revealed in our additional experiments presented in Fig. S6 in the ESI. In the recovery process, the constant hydration number around 3700 turned to decline with $T \approx$ 55°C

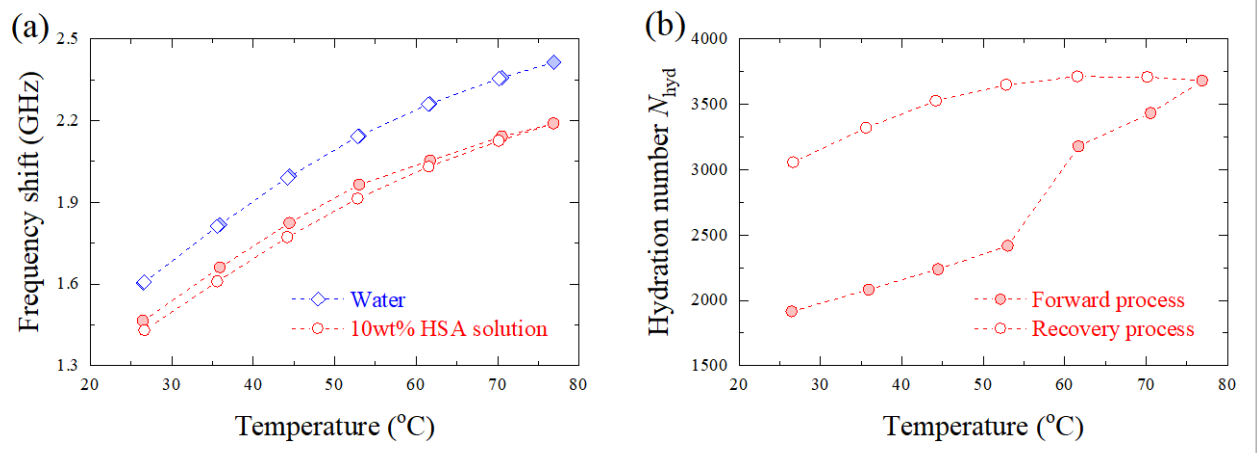

Fig. 6 (a) Temperature dependence of the frequency shift $\Delta f(T)$ of pure water and the 10 wt% HSA aqueous solution when the sample temperature shifts step-by-step up to nearly 80°C. Closed and open symbols represent the heating and cooling processes, respectively. Experimental uncertainty (typically not more than ± 0.6 MHz) is not displayed here. (b) Derived hydration number as a function of temperature, $N_{\mathrm{hvd}}(T)$, of the 10 wt% HSA aqueous solution. Closed and open circles represent the heating and cooling processes, respectively. Uncertainty is not shown because the error bars are smaller than the symbol sizes.

as a boundary, at the similar rate to that in the forward process. Since the secondary structure content is kept at constant values in this temperature range (see Fig. 3(d)), the observed decrease of N_{hyd} may be attributed to reduction in SASA without restoring the native secondary structure.

At 25°C after recovery, the hydration number N_{hyd} obtained by the "step-by-step" heating experiment was significantly larger than that by the previous "temporal" heating shown in Fig. 5(b). This discrepancy is due to a lower degree of denaturation for the latter heating treatment: according to an earlier study quantifying the degree of denaturation by measuring optical absorption of 2-(4'-hydroxyphenylazo) benzoic acid that specifically binds to the native albumin, the degree of denaturation by our "temporal" heating is about half of that by the "step-by-step" one.[98]

4. Conclusions

Although it is widely known that biological functions of proteins are built on harmonization with hydration water surrounding them, as far as the *amount* of hydration water is concerned, the commitment of hydration upon dynamical transition is yet to be described because of technical difficulties in precisely characterizing the hydration number N_{hyd}. To address this issue, this study first embarked on developing a theoretical algorithm to quantitatively determine N_{hyd} based on the frequency shift Δf of a state-of-art 65 GHz CMOS dielectric sensor. To this end, the complex dielectric function $\tilde{\varepsilon}(\omega)$ of the native HSA aqueous solution from 10 MHz to 12 THz was determined by combining five different spectroscopy systems to expose the underlying molecular mechanism that is observed around the 65 GHz region. As a consequence, we revealed that $\tilde{\varepsilon}$ around 65 GHz *selectively* reflects the reorientation dynamics of bulk water, indicating that the measured Δf by our CMOS dielectric sensor was an appropriate index to quantify the amount of bulk water. Next, by defining hydration water as any water molecule that no longer reorients as bulk, we were able to characterize the "global" hydration state, including both the tightly bound and the relatively loosely

perturbed water. The value N_{hyd} determined by our CMOS measurement was in good agreement with that obtained by dielectric spectroscopy, but the markedly reduced uncertainty (by about one-fifth) could be obviously traced back to the ultimately stable oscillation frequency of the CMOS dielectric sensor.

Benefitting from such ultimate precision, we succeeded in characterizing the transition of N_{hyd} upon thermal denaturation of HSA, with an uncertainty of ~ 1 %. The rapid rise in N_{hyd} observed at around 55°C excellently in phase with the rupture of the α-helical structure into solvent-exposed extended chains, as observed by our FTIR spectroscopy. This result indicates that the loose hydration shell at high temperatures allows the secondary and tertiary structure of protein to unfold, and the increase in the hydration number N_{hyd} arises as a consequence of the unfolded secondary structure. Owing to recent advances in molecular dynamics simulations investigating "macroscopic" thermodynamic quantities, it is reported that hydration entropy drives a protein to fold while the large amount of gain from hydration enthalpy plays a part in protein unfolding.[90,91] Remarkably, our "microscopic" observation that entropically unfavorable but energetically favorable hydration water is increased in amount upon thermal denaturation is consistent with the general view of the thermodynamic mechanisms. Further quantitative characterization of the hydration state will help to understand the biological roles of hydration water in protein folding, recognition and catalytic activity of enzymes.[99]

Conflicts of interest

The authors declare no competing financial interest.

Acknowledgements

We are grateful to Professor Toshiyuki Shikata (Tokyo University of Agriculture and Technology) and Professor Koichiro Tanaka (Kyoto University) for providing experimental apparatuses for dielectric and FTIR measurements. Financial support was provided by Industry-Academia Collaborative R&D from JST, Research Foundation for Opto-Science and Technology, RIKEN Special Postdoctoral Researcher Program and RIKEN Incentive Research Projects.

References

(1) H. Yang, G. Luo, P. Karnchanaphanurach, T.-M. Louie, I. Rech, S. Cova, L. Xun and X. S. Xie, *Science*, 2003, **302**, 262.

(2) M. Karplus and J. Kuriyan. *Proc. Natl. Aced. Sci. USA.*, 2005, **102**, 6679.

(3) K. Kuroi, K. Okajima, M. Ikeuchi, S. Tokutomi and M. Terazima, *Proc. Natl. Aced. Sci. USA.*, 2014, **111**, 14764.

(4) C. Jia, P. Xie, M. Chen and M. Q. Zhang, *Sci. Rep.*, 2017, **7**, 16037.

(5) P. Ball, *Proc. Natl. Aced. Sci. USA.*, 2017, **114**, 13327.

(6) J. A. Rupley and G. Careri, *Adv. Protein Chem.*, 1991, **41**, 37.

(7) M. M. Teeter, *Annu. Rev. Biophys. Chem.*, 1991, **20**, 577.

(8) W. Doster, S. Cusack and W. Petry, *Nature*, 1989, **337**, 754.

(9) D. Vitkup, D. Ringe, G. A. Petsko and M. Karplus, *Nat. Struct. Biol.*, 2000, **7**, 34.

(10) M. Tarek and D. J. Tobias, *Phys. Rev. Lett.*, 2002, **88**, 138101.

(11) S.-H. Chen, L. Liu, E. Frantini, P. Baglioni, A. Faraone and E. Mamontov, *Proc. Natl. Aced. Sci. USA.*, 2006, **103**, 9012.

(12) P. Kumar, Z. Yan, L. Xu, M. G. Mazza, S. V. Buldyrev, S.-H. Chen, S. Sastry and H. E. Stanley, *Phys. Rev. Lett.*, 2006, **97**, 177802.

(13) W. Doster, S. Busch, A. M. Gaspar, M.-S. Appavou, J. Wuttke and H. Scheer, *Phys. Rev. Lett.*, 2010, **104**, 098101.

(14) M. G. Mazza, K. Stokely, S. E. Pagnotta, F. Bruni, H. E. Stanley and G. Franzese, *Proc. Natl. Aced. Sci. USA.*, 2011, **108**, 19873.

(15) G. W. Robinson and C. H. Cho, *Biophys. J.*, 1999, **77**, 3311.

(16) H. Jansson and J. Swenson, *J. Chem. Phys.*, 2008, **128**, 245104.

(17) Y. Zhang, M. Lagi, D. Liu, F. Mallamace, E. Fratini, P. Baglioni, E. Mamontov, M. Hagen and S.-H. Chen, *J. Chem. Phys.*, 2009, **130**, 135101.

(18) F. Mallamace, C. Corsaro, D. Mallamace, N. Cicero, S. Vasi, G. Dugo and H. E. Stanley, *Front. Phys.*, 2015, **10**, 106104.

(19) F. Mallamace, C. Corsaro, D. Mallamace, S. Vasi, C. Vasi, H. E. Stanley and S.-H. Chen, *J. Chem. Phys.*, 2015, **142**, 215103.

(20) C. Corsano and F. Mallamace, *Physica A*, 2011, **390**, 2904.

(21) B. Meloun, L. Morávek, and V. Kostka, *FEBS Lett.*, 1975, **58**, 134.

(22) X. He and D. C. Carter, *Nature*, 1992, **358**, 209.

(23) D. C. Carter and J. X. Ho, *Adv. Protein Chem.*, 1994, **45**, 152.

(24) S. Sugio, A. Kashima, S. Mochizuki, M. Noda and K. Kobayashi, *Protein Eng.*, 1999, **12**, 439.

(25) G. A. Picó, *Int. J. Biol. Macromol.*, 1997, **20**, 63.

(26) K. Flora, J. D. Brennan, G. A. Baker, M. A. Doody and F. V. Bright, *Biophys. J.*, 1998, **75**,1084.

(27) S. S. Krishnakumar and D. Panda, *Biochem.*, 2002, **41**, 7443.

(28) M. Rezaei-Tavirani, S. H. Moghaddamnia, B. Ranjbar, M. Amani and S.-A. Marashi, *J. Biochem. Mol. Biol.*, 2006, **39**, 530.

(29) V. M. Rosenoer, M. Oratz and M. A. Rothchild, *Albumin Structure, Function and Uses*. Pergamon, Oxford, 27-51, 1977.

(30) J. Pérez, J.-C. Zanotti and D.Durand, *Biophys. J.*, 1999, **77**, 454.

(31) K. Yokoyama, T. Kamei, H. Minami and M. Suzuki, *J. Phys. Chem. B*, 2001, **105**, 12622.

(32) A. Oleinikova, P. Sasisanker and H. Weingärtner, *J. Phys. Chem. B*, 2004, **108**, 8467.

(33) C. Cametti, S. Marchetti, C. M. C. Gambi and G. Onori, *J. Phys. Chem. B*, 2011, **115**, 7144.

(34) M. Wolf, R. Guilich, P. Lunkenheimer and A. Loidl, *Biochim. Biophys. Acta.*, 2012, **1824**, 723.

(35) U. Raveendrananth, S. Bijukumar and K. T. Mathew, *IEEE Trans. Instrum. Meas.*, 2000, **49**,1305.

(36) W. Xu, L. Xie and Y. Ying, *Nanoscale*, 2017, **9**, 13864.

(37) A. Réjou-Michel, F. Henry, M. de Villardi and M. Delmotte, *Phys. Med. Biol.*, 1985, **30**, 831.

(38) T. Mitsunaka, D. Sato, N. Ashida, A. Saito, K. Iizuka, T. Suzuki, Y. Ogawa and M. Fujishima,

IEEE J. Solid-State Circuits, 2016, **51**, 2534.

(39) J. Grzyb, B. Heinemann and U.R. Pfeiffer, *IEEE J. Solid-State Circuits*, 2016, **51**, 3063.

(40) K. Entesari, A. A. Helmy and M. Moslehi-Bajestan, *IEEE Microw. Mag.*, 2017, **18**, 57.

(41) K. Arai and T. Shikata, *Phys. Chem. Chem. Phys.*, 2019, **21**, 25379.

(42) K. Shiraga, K. Tanaka, T. Arikawa, S. Saito and Y. Ogawa, P*hys. Chem. Chem. Phys.*, 2018, **20**, 26200.

(43) J. E. Bertie and Z. Lan, *J. Chem. Phys.*, 1996, **105**, 8502.

(44) J. Grdadolnik, *Acta. Chim. Slov.*, 2002, **49**, 631.

(45) A. Barth, *Biochim. Biophys. Acta*, 2007, **1767**, 1073.

(46) R. Buchner, J. Barthel and J. Stauber, *Chem. Phys. Lett.*, 1999, **306**, 57.

(47) D. M. Leitner, M. Gruebele and M. Havenith, *HFSP J.*, 2008, **2**, 314.

(48) Y. He, P. I. Ku, J. R. Knab, J. Y. Chen, and A. G. Markelz, *Phys. Rev. Lett.*, 2008, **101**, 178103.

(49) K. Shiraga, Y. Ogawa and N. Kondo, *Biophys. J.*, 2016, **111**, 2629.

(50) K. Shiraga, A. Adachi, M. Nakamura, T. Tajima, K. Ajito and Y. Ogawa, *J. Chem. Phys.*, 2017, **146**, 105102.

(51) K. Shiraga, Y. Ogawa, K. Tanaka, T. Arikawa, N. Yoshikawa, M. Nakamura, K. Ajito and T. Tajima, *J. Phys. Chem B*, 2018, **122**, 1268.

(52) D. Bendedouch and S.-H. Chen, *J. Phys. Chem.*, 1983, **87**, 1473.

(53) F. Zhang, F. Roosen-Runge, M. W. A. Skoda, R. M. J. Jacobs, M. Wolf, P. Callow, H. Frielinghaus, V. Pipich, S. Prévost and F. Schreiber, *Phys. Chem. Chem. Phys.*, 2012, **14**, 2483.

(54) D. Braun, M. Schmollngruber and O. Steinhauser, *Phys. Chem. Chem. Phys.*, 2017, **19**, 26980.

(55) Z. Cao and J. U. Bowie, *Protein Sci.*, 2014, **23**, 566.

(56) D. M. Byler and H. Susi, *Biopolymers*, 1986, **25**, 469.

(57) E. Bramanti and E. Benedetti, *Biopolymers*, 1996, **38**, 639.

(58) J. Grdadolnik and Y. Maréchal, *Biopolymers*, 2001, **62**, 54.

(59) D. Usoltsev, V. Sitnikova, A. Kajava and M. Uspenskaya, *Biomolecules*, 2019, **9**, 359.

(60) H. Huang, J. Xie and H. Chen, *Analyst*, 2011, **136**, 1747.

(61) E. S. Manas, Z. Getahun, W. W. Wright, W. F. DeGrado and J. M. Vanderkooi, *J. Am. Chem. Soc.*, 2000, **122**, 9883.

(62) V. A. Lórenz-Fonfría, C. Bamann, T. Resler, R. Schlesinger, E. Bamberg and J. Heberle, *Proc. Natl. Aced. Sci. USA.*, 2015, **112**, E5796.

(63) H. Torii, *J. Phys. Chem. Lett.*, 2015. **6**, 727.

(64) T. Lefévre, K. Arseneault and M. Pézolet, *Biopolymers*, 2004, **73**, 705.

(65) X. Zhou, Z. He and H. Huang, *Vib. Spectrosc.*, 2017, **92**, 273.

(66) I. Noda, A. E. Dowrey, C. Marcott, G. M. Story and Y. Ozaki, *Appl. Spectrosc.*, 2000, **54**, 236A.

(67) K. Shiraga, A. Adachi and Y. Ogawa, *Chem. Phys. Lett.* 2017, **678**, 59.

(68) E. Goormaghigh, J.-M. Ruysschaert and V. Raussens, *Biophys. J.*, 2006, **90**, 2946.

(69) S.-Y. Lin, K.-S. Chen and L. Run-Chu, *Polymer*, 1999, **40**, 2619.

(70) Y. Maeda, T. Higuchi and I. Ikeda, *Langumuir*, 2000, **16**, 7503.

(71) B. Sun, Y. Lin, P. Wu and H. W. Siesler, *Macromolecules*, 2008, **41**, 1512.

(72) S. Gnanakaran and R. M. Hochstrasser, *J. Am. Chem. Soc.*, 2001, **123**, 12886.

(73) S. Morita, H. Shinzawa, R. Tsenkova, I. Noda and Y. Ozaki, *J. Mol. Struc.*, 2006, **799**, 111.

(74) R. K. Mitra, S. S. Sinha and S. K. Pal, *Langmuir*, 2007, **23**, 20224.

(75) Y. Moriyama, E. Watanabe, K. Kobayashi, H. Harano, E. Inui and K. Takeda, *J. Phys. Chem. B*, 2008, **112**, 16585.

(76) T. Q. Luong, P. K. Verma, R. K. Mitra and M. Havenith, *Biophys. J.*, 2011, **101**, 925.

(77) L. Fu, S. Villette, S. Petoud, F. Fernandez-Alonso and M.-L. Saboungi, *J. Phys. Chem. B*, 2011, **115**, 1881.

(78) Y. Sun, T. Ishida and S. Hayakawa, *J. Agric. Food. Chem.*, 2004, **52**, 2351.

(79) D. Poeter and F. Vollrath, *Biochim. Biophys. Acta*, 2012, **1824**, 785.

(80) D. I. Svergun, S. Richard, M. H. J. Koch, Z. Sayers, S. Kuprin and G. Zaccai, *Proc. Natl. Acad. Sci. USA.*, 1998, **95**, 2267.

(81) F. Merzel and J. C. Smith, *Proc. Natl. Acad. Sci. USA.*, 2002, **99**, 5378.

(82) M. Heyden, *J. Chem. Phys.*, 2019, **150**, 094701.

(83) N. Sengupta, S. Jaud and D. J. Tobias, *Biophys. J.*, 2008, **95**, 5257.

(84) D. C. Elton, *Phys. Chem. Chem. Phys.*, 2017, **19**, 18739.

(85) R. Schulz, Y. von Hansen, J. O. Daldrop, J. Kappler, F. Noé and R. R. Netz, *J. Chem. Phys.*, 2018, **149**, 244504.

(86) S. Seyedi and D. V. Matyushov, *Chem. Phys. Lett.*, 2018, **713**, 210.

(87) Y. Qin, L. Zhang, L. Wang and D. Zhong, *J. Phys. Chem. Lett.*, 2017, **8**, 1124.

(88) D. R. Martin and D. V. Matyushov, *J. Chem. Phys.*, 2014, **141**, 22D501.

(89) G. Bellavia, L. Puccou, S. Achir, Y. Guinet, J. Siepmann and A. Hédoux, *Food Biophys.*, 2013,

8, 170.

(90) T. Yoshidome, M. Kinoshita, S. Hirota, N. Baden and M. Terazima, *J. Chem. Phys.*, 2008, **128**, 225104.

(91) Y. Maruyama and Y. Harano, *Chem. Phys. Lett.*, 2013, **581**, 85.

(92) D. Mallamace, E. Fazion, F. Mallamace and C. Corsaro, *Int. J. Mol. Sci.*, 2018, **19**, 3825.

(93) O. S. Nnyigide, S.-G. Lee and K. Hyun, *J. Mol. Model.*, 2018, **24**, 75.

(94) M. Hennig, F. Roosen-Runge, F. Zhang, M. Zorn, M. W. A. Sokoda, R. M. J. Jacobs, T. Seydel and F. Schreiber, *Soft Matter*, 2012, **8**, 1628.

(95) M. Grimaldo, F. Roosen-Runge, M. Hennig, F. Zanini, F. Zhang, N. Jalarvo, M. Zamponi, F. Schreiber and T. Seydel, *Phys. Chem. Chem. Phys.*, 2015, **17**, 4645.

(96) Y. Gavrilov, J. D. Keuchter and Y. Levy, *Phys. Chem. Chem. Phys.*, 2017, **19**, 8243.

(97) S. Pal, K. Chakraborty, P. Khatua and S. Bandyopadhyay, *J. Chem. Phys.*, 2015, **142**, 055102.

(98) M. Nakagaki and Y. Sano, *Bull. Chem. Soc. Japan*, 1972, **46**, 791.

(99) Y. Levy and J. N. Onuchi, *Annu. Rev. Biophys. Biomol. Struct.*, 2006, **35**, 389.